BULLETIN OF THE POLISH ACADEMY OF SCIENCES
TECHNICAL SCIENCES, Vol. 69(4), 2021, Article number: e137936
DOI: 10.24425/bpasts.2021.137936

Modeling and parametric optimization of friction stir welding of aluminium alloy AA7068-T6 using response surface methodology and desirability function analysis

Bindu M D[1*], Tide P S[1], Bhasi A B[1], and Ramachandran K K[2]

[1] Division of Mechanical Engineering, Cochin University of Science and Technology, Kerala, India
[2] Department of Mechanical Engineering, Government Engineering College, Trissur, Kerala, India

Abstract. In this investigation, high specific strength precipitation hardenable alloy AA7068-T6 was joined using friction stir welding. Experiments were carried out using the three factor-three level central composite face-centered design of response surface methodology. Regression models were developed to assess the influence of tool rotational speed, welding speed, and axial force on ultimate tensile strength and elongation of the fabricated joints. The validity of the developed models was tested using the analysis of variance (ANOVA), actual and adjusted values of the regression coefficients, and experimental trials. The analysis of the developed models together with microstructural studies of typical cases showed that the tool rotational speed and welding speed have a significant interaction effect on the tensile strength and elongation of the joints. However, the axial force has a relatively low interaction effect with tool rotational speed and welding speed on the strength and elongation of the joints. The process variables were optimized using the desirability function analysis. The optimized values of joint tensile strength and elongation – 516 MPa and 21.57%, respectively were obtained at a tool rotational speed of 1218 rpm, welding speed of 47 mm/min, and an axial force of 5.3 kN.

Key words: AA7068-T6; friction stir welding; response surface method; desirability function.

1. INTRODUCTION

Aluminium-zinc alloy, AA7068 is a potential material in aerospace applications due to its extremely high strength-to-weight ratio [1]. Currently it is used for the manufacturing of connecting rods, engine shafts and valve components. Joining this precipitation hardenable alloy by traditional or even advanced fusion welding techniques is quite difficult. Fusion welding of the 7xxx alloys develops defects like hot cracking and porosity in the weld zone. Also, significant loss of mechanical and corrosion properties is observed in the 7xxx alloy weld joints after fusion welding. Besides, the vaporization of zinc in Al-Zn alloys during fusion welding creates health hazards [2]. Riveting and mechanical fastening are costly and add weight to the structure. The application spectrum of AA 7068 can be widened if a suitable joining method is devised. Friction stir welding (FSW) is a solid-state welding technique developed at The Welding Institute (TWI), UK in 1991 for the joining of aluminium alloys. FSW can eliminate all problems associated with melting and solidification phases in fusion welding processes. Most metals and alloys, a few non-metals and dissimilar materials can be efficiently joined by FSW technique [3]. During the FSW of similar materials, the process variables control the joint quality are: the tool rotational speed, welding speed, axial force, tool material and tool geometry [4–7]. While joining dissimilar materials, the tool tilt angle, relative position of the materials and tool offset are also important factors that control the heat input, material flow and joint integrity [8]. Successful joining by FSW is largely dependent on the selection of the best possible combination of the above-mentioned process variables. However, the selection of FSW parameter combination that provides acceptable weld quality is resource-intensive as it involves extensive experimental trials. It is established that the use of statistical DOE techniques together with regression modeling can reduce the resources involved in experimental investigations, without sacrificing accuracy. Response surface methodology (RSM) is effectively utilized in the investigations on welding and joining including FSW recently [9, 10]. The RSM-DOE techniques are inherently capable to develop second degree polynomial models for the responses wherein the response is a function of several variables. The weld quality is often evaluated in terms of the tensile strength, hardness, ductility, corrosion resistance, etc. of the joints and is mostly interdependent. Taking these variables as responses, a welding problem essentially is a multi-response problem. Deepandurai and Parameswaran [11] used RSM with fuzzy Grey relational analysis for the multi-response optimization of FSW of AA7075 with SiC reinforcements and reported close agreement with experimental measurements. RSM with ANN methodology was used effectively for the multi- response optimization of dissimilar welding [12]. For the optimization of multi-response problems, the desirability

*e-mail: mdbindudharmajan@gmail.com

Manuscript submitted 2020-06-02, revised 2021-05-16, initially accepted for publication 2021-06-09, published in August 2021

function approach is known to be one of the very efficient and straightforward methods [13].

Based on the extensive literature scrutiny, to the best of knowledge of the authors, no investigation on FSW of AA7068 aluminium alloy with or without RSM-based modeling and optimization is reported in the literature. Also, in the reported works on FSW of other 7xxx aluminium alloys, the investigation is carried out with randomly selected process parameters and mostly the axial force – an important FSW parameter – is not even considered as a controlled parameter. Therefore in the present study, aluminium alloy AA7068-T6 was friction stir welded using the RSM-central composite face centered experimental design with the tool rotational speed, welding speed and axial force as variables. Afterwards, response surface polynomial models were developed for the tensile properties of the joints and multi-objective parametric optimization of the FSW process was carried out using the desirability function analysis.

2. MATERIALS AND METHODS

2.1. Selection of FSW variables and preparation of DOE matrix

The primary FSW parameters; tool rotational speed (N), welding speed (S) and axial force (F) are considered as the variables (factors) for the present investigation. The ultimate tensile strength (UTS) and percentage elongation of the welded joints are the assessed responses. The central composite face-centered (CCF) variant of the RSM design was the DOE technique applied for the experimental trials. The variables in coded form for the CCF design and their corresponding actual values are shown in Table 1. The three factor-three level CCF design has 20 runs, comprising of six star points, six center points, and eight runs of factorial points. The experimental FS welding trials were performed by completely randomizing the developed design matrix.

Table 1
Coded levels for the RSM-CCF design and the corresponding actual values of variables

Factor Parameters	Symbol	Levels		
		–1	0	1
Tool Rotational Speed (RPM)	*N*	800	1100	1400
Welding speed (mm/min)	*S*	30	45	60
Axial Force (kN)	*F*	5	7	9

2.2. Experimental details

Commercially available AA7068-T6 aluminium alloy sheet with 6 mm thickness was used as the base material. The chemical composition of the base metal is given in Table 2. The tensile strength of base metal is 586 MPa and elongation is 11%. Work pieces with dimensions of 100 mm×50 mm×6 mm were prepared using a shearing machine.

The FSW tool with featureless shoulder and cylindrical pin, made of H13 tool steel having shoulder diameter of 20 mm, pin diameter of 6 mm and pin length of 5.7 mm was used for the trials. A photographic image of the FSW tool is shown in Fig. 1.

Table 2
Chemical composition of AA 7068-T6

Chemical composition			
Element	wt.%	Element	wt.%
Si	0.14	Cr	0.05
Fe	0.19	Ni	0.007
Cu	2.4	Zn	8.3
Mn	0.03	Ti	0.05
Mg	3.03	Al	85.51

The welding of the work pieces was carried out in the butt-joint configuration using a dedicated semi-automatic friction stir welding machine with 60 kN capacity (Fig. 2). The fabricated joints are depicted in Fig. 3. The UTS and elongation of the welded samples were assessed using a computer-controlled electromechanical universal testing machine with 25 kN capacity at a crosshead speed of 4 mm/min.

Fig. 1. FSW tool

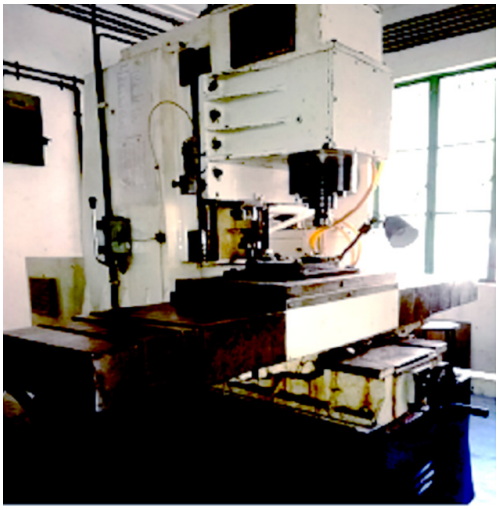

Fig. 2. FSW machine

Fig. 3. Fabricated joints

Two tensile specimens each, as per ASTM E8-M08 standard, were prepared from every welded sample using the wire-cut EDM process. A typical set of tensile specimens extracted from the welded joints is shown in Fig. 4.

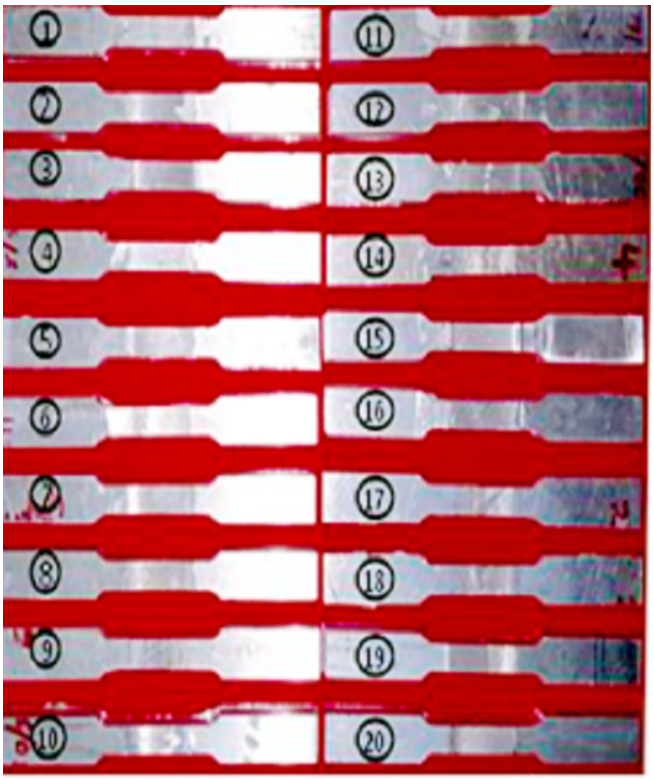

Fig. 4. Typical set of tensile specimens extracted from the welded joints

The average value of the ultimate tensile strength and percentage elongation of the two specimens were calculated. For the purpose of correlating the effect of FSW parameters on the responses, the weld zone of joints produced at selected runs was examined using optical microscopy (OM). For OM, the specimens extracted across the joint line were polished following standard metallographic specimen preparation procedure and etched using Keller's reagent. The etched specimens were observed under metallographic microscope Olympus BX51M, at different magnifications.

2.3. Development of mathematical model

The generalized form of the second order response surface model is given below:

$$Y = b_0 + \sum_{i=1}^{k} b_i x_i + \sum_{i=1}^{k} b_{ii} x_i^2 + \sum_{i=1}^{k-1} \sum_{j=i+1}^{k} b_{ij} x_i x_j, \qquad (1)$$

where y is the predicted response, b_0, b_i, b_{ii} and b_{ij} are coefficients whose magnitudes depend on the magnitude of the respective responses and the individual and interaction effects of the variables x_i and x_j. The second order standard polynomial model for the UTS and elongation in terms of the three factors N, S and F are given below:

$$UTS = b_0 + b_1 N + b_2 S + b_3 F + b_{11} N^2 + b_{22} S^2 + b_{33} F^2 + b_{12} \times N \times S + b_{13} \times N \times F + b_{23} \times S \times F, \qquad (2)$$

$$E = b_0 + b_1 N + b_2 S + b_3 F + b_{11} N^2 + b_{22} S^2 + b_{33} F^2 + b_{12} \times N \times S + b_{13} \times N \times F + b_{23} \times S \times F. \qquad (3)$$

The average values of responses, UTS and elongation, obtained for the FS weld joints fabricated as per the randomized DoE matrix are shown in Table 3. The RSM models for the observed values of responses in terms of the three variables were developed using a proprietary statistical software. The coefficients of the models were tested for their significance at 95% confidence level by applying student's t-test. The final RSM model, after eliminating statistically insignificant terms by the step by step method, is given below:

$$UTS = 498.7 - 3.20 \times S - 9.3 \times F + 14.8 \times N - 102.88S^2 - 47.87N^2 + 25.75 \times N \times S - 35 \times N \times F \quad \text{(MPa)}, \qquad (4)$$

$$E = 21.162 + 1.015 \times N + 0.736 \times S + 0.971 \times F - 2.697N^2 - 4.502F^2 + 0.521 \times N \times S - 1.006 \times N \times F \quad (\%). \qquad (5)$$

2.4. Adequacy tests and validation of the model

The adequacy of the developed regression models was assured by the analysis of variance (ANOVA) and the value of coefficient of determination (R^2). The results of the ANOVA for UTS and elongation are shown in Table 4 and Table 5, respectively. The larger F-values and very low probability values (equal to zero for UTS model and almost zero for the elongation model) at 95% confidence level indicate that the models are adequate and capable to predict the responses, UTS and % elongation, accurately. The actual and adjusted R^2 values of the model for UTS are 0.979 and 0.967, respectively and that for elongation

Table 3
RSM-CCF design matrix with and actual values of variables and values of responses in each experimental run

Actual values of the factors			Responses	
Tool Rotational Speed (N)	Welding Speed (S)	Axial Force (F)	Tensile Strength	Elongation
rpm	mm/min	kN	MPa	%
1400	30	7	495	20.56
1100	45	5	321	12.50
1100	45	5	516	21.67
1400	60	7	380	16.80
1100	45	7	290	10.56
800	30	5	410	16.39
1400	45	5	455	19.44
1400	30	7	445	17.36
800	45	7	486	19.44
1100	45	7	499	20.83
1100	45	9	289	11.94
800	60	7	512	21.67
1100	30	7	350	13.06
1100	45	5	479	20.56
1100	45	9	390	14.44
800	60	9	324	11.94
1100	60	7	390	11.11
1100	45	9	432	17.50
1400	60	7	489	20.83
800	30	9	516	21.67

Table 4
ANOVA of the developed model – UTS

Model for UTS				
Source	Sum of Squares (SS)	Mean Squares	F-Value	P-Value
Regression	112189	16027.1	79.76	0
N^2	7334	7334.5	36.5	0
S^2	33866	33866.4	168.54	0
F^2	–	–	–	–
$N \times S$	5305	5304.5	26.4	0
$N \times F$	9800	9800	48.77	0

Table 5
ANOVA of the developed model – Elongation

Model for Elongation				
Source	Sum of Squares (SS)	Mean Squares	F-Value	P-Value
Regression	299.433	37.4291	133.92	0
N^2	20.007	20.007	71.58	0
S^2	55.744	55.7438	199.44	0
F^2	3.311	3.311	11.85	0.006
$N \times S$	2.174	2.1736	7.78	0.018
$N \times F$	8.1	8.1003	28.98	0

are 0.989 and 0.982, respectively. Considering the uncertainty associated with the responses and variables of the model, the R^2 values indicate excellent fit of the experimental data. The scatter plot shown in Fig. 5 also demonstrates accurate fit of the experimental data as the actual responses are distributed very close to the line of predicted responses.

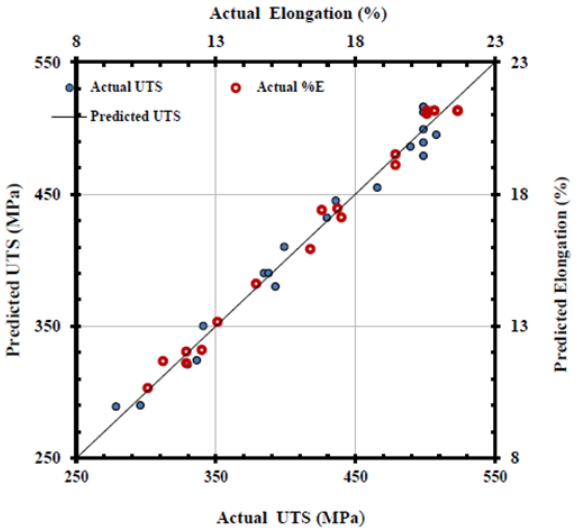

Fig. 5. Scatter plot of UTS and elongation

In addition, the mathematical models were experimentally validated by comparing the responses obtained in the welding trials conducted at four randomly selected parametric combinations with that computed by the models. The experimentally obtained values of responses were in agreement with the computed values and have an average error of 3.4% and 2.8% for the UTS and elongation, respectively.

2.5. Multi-response optimization using the desirability analysis

Desirability function analysis is a statistical technique that transforms a multi-response optimization problem into a single response problem using mathematical transformations [14]. In this approach, each response y_i is assigned a dimensionless desirability function $d_i(y_i)$, whose magnitude is such that $0 \leq d_i(y_i) \leq 1$. A $d_i(y_i)$ value of zero indicates that the response is completely undesirable, whereas, $d_i(y_i)$ equal to one indicates the response is completely desirable. The geometric mean of individual desirability values of each of the responses is the overall desirability function D calculated as in equation (6).

$$D = \left[d_1(y_1) \times d_2(y_2) \times \ldots \times d_n(y_n)\right]^{\frac{1}{n}}, \tag{6}$$

where n is the number of responses (y_i) involved in the optimization problem. In a particular optimization problem, the responses can be maximized, minimized or can be assigned a target value, depending on the nature of the process and the responses involved. The desirability function $d_i(y_i)$ used will be different for different types of optimization problems. In this investigation, since both the responses (UTS and elongation) are to be maximized, the desirability function given in equation (7) is utilized.

$$d_i y_i = \begin{cases} 0 & \text{if } y_i < y_{\min} \\ \dfrac{y_i - y_{\min}}{y_{\max} - y_{\min}} & \text{if } y_{\min} \le y_i \le y_{\max} \\ 1 & \text{if } y_i > y_{\min} \end{cases}. \quad (7)$$

y_i is the response and $y_{\min}$ and $y_{\max}$ are the lower and upper limits of the response y_i. The multi-response optimization of the FSW process using desirability function approach, stated above, was carried out using the 'response optimizer' option in the proprietary statistical software.

3. RESULTS AND DISCUSSION

3.1. Influence of FSW parameters on UTS and elongation of the joints

It is established that in the FSW of similar and dissimilar materials, the tool rotational speed, welding speed and axial force have a significant influence on the joint properties, individually [15, 16]. With regard to combined (interaction) effect of FSW parameters, conflicting arguments are available in the literature. Thus, the statistically and experimentally validated mathematical models for the UTS and elongation were analyzed to study and rationalize the influence of FSW variables on the tensile properties-UTS and elongation, of the joints.

3.1.1. Influence of tool rotational speed on UTS and elongation of the joints

The effect of tool rotational speed on UTS and elongation of the joints is illustrated in Figs. 6(a) and (b), respectively. The model predicts peak values of tensile strength at tool rotational speed in the range of 1100–1400 rpm (at a welding speed of 45 mm/min and an axial force of 5 kN). The lowest joint strength of about 70% of the UTS of the base alloy is observed at tool rotational speed of 800 rpm, welding speed of 45 mm/min and axial force of 5 kN. At axial forces of 5 kN and 7 kN, the elongation of the joints also follow a similar variation as that of the UTS within the entire range of tool rotational speed experimented. However, towards lower tool rotational speeds and an axial force of 9 kN, the elongation of the joints is relatively less than that at other parameter combinations. Also, from the nature of variability of the individual plots, it can be seen that both the tool rotational speed and welding speed have significant interaction effect on the UTS and elongation of the joints.

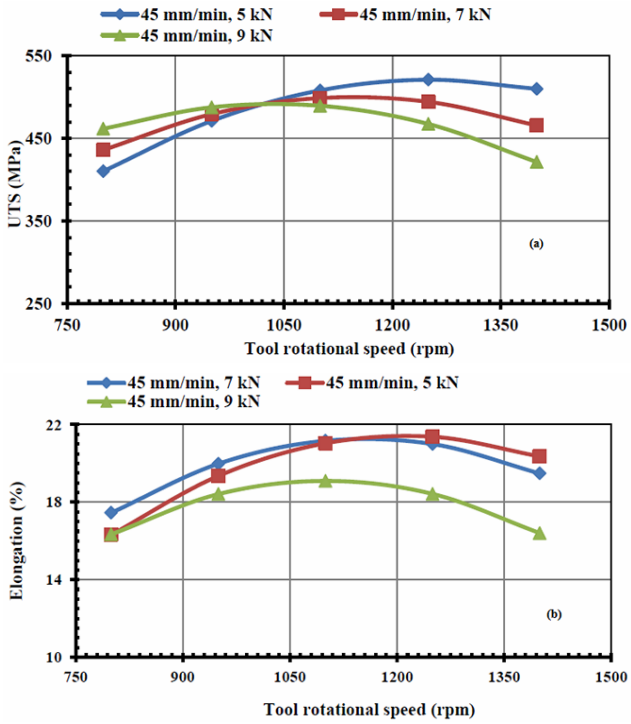

Fig. 6. Effect of tool rotational speed on (a) UTS (b) Elongation of the joints

Figure 7 shows the optical micrograph of the SZ and thermomechanically affected zone (TMAZ) of a typical joint fabricated at a tool rotational speed of 1250 rpm, welding speed of 45 mm/min and an axial force of 5 kN. This joint has exhibited the highest joint strength of 518.45 MPa with an elongation of 21.2%. In Fig. 8(a), in the optical micrograph of the base metal the strengthening precipitate in the AA7068-T6 base aluminum alloy-the coherent 'η' phase [17] is seen distributed in the aluminium matrix. Figure 7 clearly shows these precipitates are broken down in the NZ by the stirring action of the tool pin. The relatively fine particles are homogeneously distributed in the matrix of recrystallized fine-grained aluminium. At the TMAZ, the grain and precipitates are deformed and coarsened due to the mechanical and thermal effects. As the tensile specimen was fractured at the interface of TMAZ and HAZ, it is obvious that the SZ and TMAZ are relatively stronger owing to the finer grain structure.

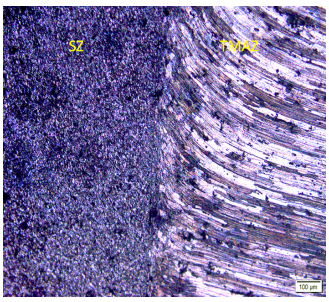

Fig. 7. Optical micrograph of NZ and TMAZ of joints fabricated at 1250 rpm, 45 mm/min and 5 kN

Optical micrograph of the HAZ of the joint is shown in Fig. 8(b). At temperatures above 350°C the precipitates dissolve and grain growth occurs in precipitation hardened alloys. As a result hardness and strength decreases [18–20]. For 7xxx alloys at peak aged condition (T6), the precipitates in the HAZ get coarsened and hence exhibit lesser hardness and strength relative to the base metal [20]. Referring to Fig. 8, it is evident

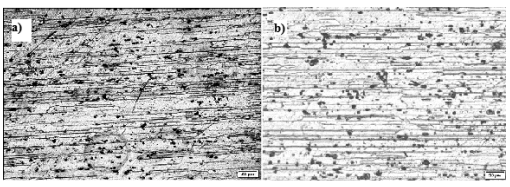

Fig. 8. Optical micrographs of: (a) Base material (b) HAZ of joint fabricated at 1250 rpm, 45 mm/min and 5 kN

that there is some amount of coarsening of grains and precipitates at the HAZ.

Figure 9 shows the optical micrograph of the weld SZ and TMAZ of a joint fabricated at tool rotational speed of 1400 rpm, welding speed of 45 mm/min and an axial force of 9 kN (joint that exhibited the lowest joint strength at higher heat input). The heat input corresponding to the given parameter combination is 3389 J/mm [21]. Some amount of coarsening of grains and precipitates has occurred at the SZ, but the precipitates are almost uniformly distributed in the SZ. From Fig. 9 it is evident that the grains and precipitates in TMAZ are subjected to appreciable amount of deformation and coarsening. The above observations explicitly make it clear that the peak temperature experienced in the weld zone is very high.

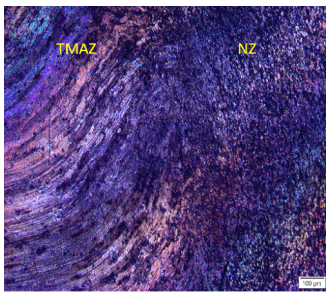

Fig. 9. Optical micrograph of joints fabricated at 1400 rpm, 45 mm/min and 9 kN

Typical optical micrographs of the HAZ of the joint produced at 1400 rpm, 45 mm/min and 9 kN and 800 rpm, 45 mm/min and 5 kN are shown in Figs. 10(a) and (b). Appreciable amount of coarsening of grains and precipitates can be observed at the HAZ which may be the reason of lower strength.

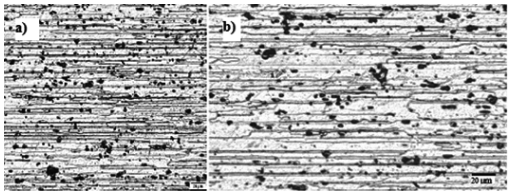

Fig. 10. Optical micrographs of HAZ of the joint fabricated at: (a) 1400 rpm, 45 mm/min and 9 kN (b) 800 rpm, 45 mm/min and 5 kN

Figure 11 shows optical micrograph of SZ and TMAZ of the joint fabricated at tool rotational speed of 800 rpm, welding speed of 45 mm/min and axial force of 5 kN. The heat input corresponding to this parameter combination is found to be 1076 J/mm [21]. At the SZ, the grains and precipitates are very fine with near homogeneous but less dense distribution of precipitates in the matrix is seen in the matrix. The grains and precipitates in the TMAZ are subjected to severe deformation but the coarsening is apparently limited.

The contour plots of both the UTS and elongation, against tool rotational speed and welding speed, shown in Figs. 12(a) and (b) are of the peaking type. The nature of contour plot indicates that a unique maximum exists for both the UTS and % elongation within the domain of the FSW parameters. Also,

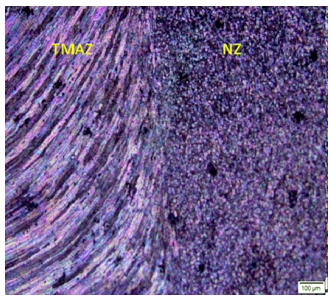

Fig. 11. Optical micrograph of joints fabricated at 800 rpm, 45 mm/min and 5 kN

considering a minimum acceptable target value of UTS as 70% of the UTS of the base metal, a wider welding parameter window (the entire range of all the welding parameters) could produce weld joints with acceptable weld strength and ductility.

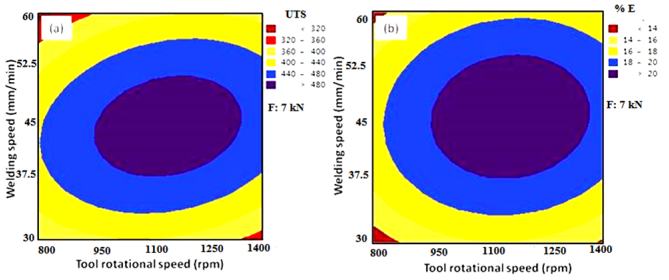

Fig. 12. Contour plot of: (a) UTS vs. tool rotational speed and welding speed (b) Elongation vs. tool rotational speed and welding speed

3.1.2. Influence of welding speed on UTS and elongation of the joints

The influence of welding speed on the UTS and elongation of the joint is portrayed in Figs. 13(a) and (b). Both the UTS and elongation follow approximately similar type of variation against welding speed and axial force. The peak values of UTS and elongation are predicted for the joint welded at 45 mm/min and 5 kN axial force (at the central value of 1100 rpm). On either side of the peak point, the UTS and elongation show gradually decreasing but symmetrical trend with the lowest values of UTS at 30 mm/min and 9 kN at the lower welding speed side and 60 mm/min and 9 kN at the higher welding speed side. At higher axial force, the elongation of the joint is relatively smaller with more proportionate reduction at lower welding speeds. This may be due to the coarsening of precipitates at the higher peak temperature with low rate of cooling resulting from the very high heat generation at low welding speeds and a high axial force of 9 kN (e.g., 3994 J/mm at 1100 rpm, 30 mm/min and 9 kN [21]. The heat generation corresponding to 1100 rpm, 45 mm/min and 5 kN (highest joint strength of 508 MPa) is 1480 J/mm. As discussed above, the peak temperature at this heat generation and cooling rate at this welding speed could be sufficient enough to cause solution heat treatment at the weld zone but not severe enough to cause coarsening of grains and precipitates at the HAZ. As the plots at different axial forces are approximately analogous (not crossing each other), it is apparent that the welding speed and ax-

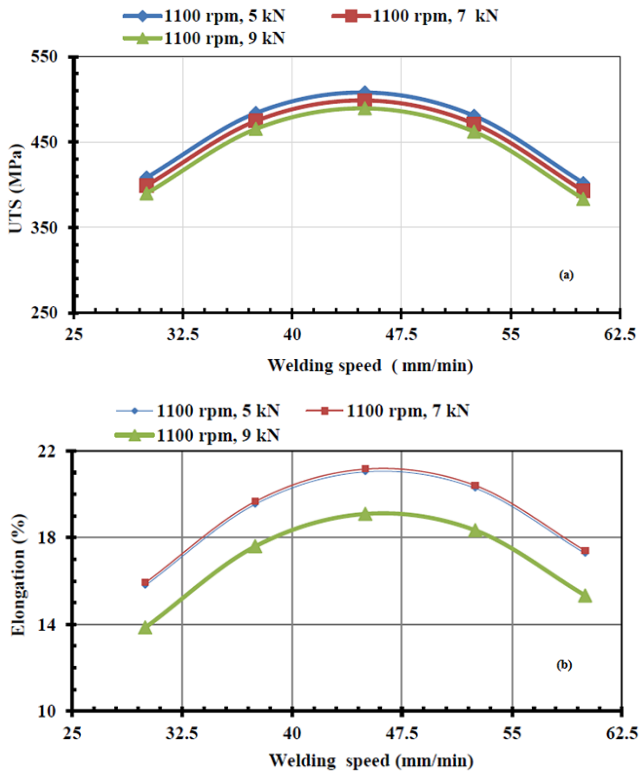

Fig. 13. Effect of Welding speed on (a) UTS (b) Elongation of the joints

ial force have no significant interaction effect on the UTS and elongation of the joints. It is a well-established fact in FSW that welding speed has an influence on the heat generation and strain rate of the material whereas axial force has an influence on the heat generation and coalescence of the material. Moreover, the welding speed and axial force have a significant interaction effect on the UTS of the FS welded joints [22]. Thus, the observed near independence of welding speed and axial force on the UTS of the joints seems slightly inconsistent. This may be the results of an unintentional shortcoming in the experimental trials that the Z-axis mechanical stopper used to safeguard the work fixture/backup plate from possible damage (in the event of excessive tool plunge) would have had a restricting effect on the applied Z-axis force.

Figures 14(a) and (b) show the contour plots of both the UTS and elongation versus axial force and welding speed. Referring to Fig. 14(a), it can be seen that the UTS neither follows a saddle type variation nor exactly the peaking type. The saddle type variation is characterized by the existence of multiple peaks in

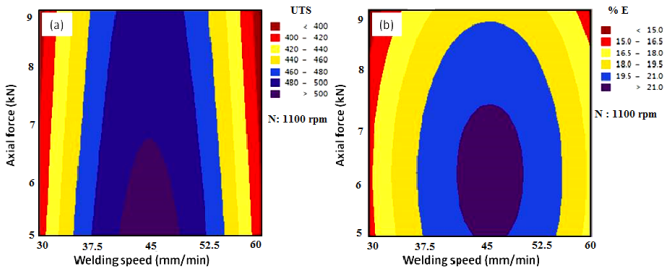

Fig. 14. Contour plot of: (a) UTS vs. welding speed and axial force (b) Elongation vs. welding speed and axial force

the experimental domain against a unique peak in the case of peaking type. This may be probably caused due to the selection of the range of axial force slightly towards the upper side, rather than a characteristic of the FSW process. In the case of elongation, the variation is clearly of the peaking type as shown in Fig. 14(b). This inconsistency in the nature of variation in UTS and ductility is probably caused due to the fracture of the joint at the interface of TMAZ and HAZ as a result of the very low material coalescence at low heat input welding conditions, described above.

3.1.3. Influence of axial force on UTS and elongation of the joints

The effect of axial force on UTS and elongation of the joints is portrayed in Figs. 15(a) and (b), respectively.

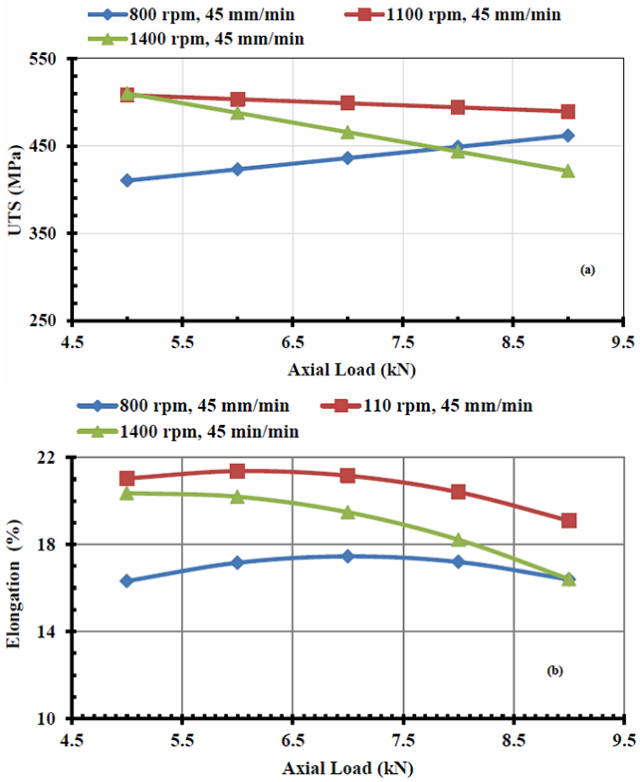

Fig. 15. Effect of axial force on (a) UTS; (b) Elongation of the joints

The UTS shows a near-linear variation against axial force at different tool rotational speeds as depicted in Fig. 15(a). At higher tool rotational speeds, low values of axial force predicts higher joint strength, whereas at low rotational speed of 800 rpm, higher UTS is predicted at higher values of axial force. The highest value of UTS of 510 MPa is predicted for joint fabricated at 1400 rpm, 45 mm/min and 5 kN. Also, within the entire range of axial force, joints with acceptable joint strength can be created at rotational speed in the range of 1100–1400 rpm with a welding speed of 45 mm/min. However, at 800 rpm and 45 mm/min, axial force in the range of 6–9 kN could only produce joints with acceptable joint strength. Figure 15(b) shows the effect of axial force on the ductility of the joints. At higher axial forces, the elongation of the joints is rela-

tively lesser. The heat generation at the parameter combination (1400 rpm, 45 mm/min and 5 kN) that predicted the highest joint strength is 1883 J/mm. The higher strength may be due to the fact that the peak temperature corresponding to the heat generation and the cooling rate at 45 mm/min would be sufficient enough to cause solution heat treatment at the weld zone but not high enough to cause excessive coarsening of grain and secondary phases at the HAZ. The nature of individual plots reveal that the axial force and tool rotational speed have appreciable interaction effect on the UTS and elongation of the joints. Though the joint strength is low at higher heat input conditions, probably due to the coarsening of precipitates and grain at the HAZ, the solution heat treatment at the weld nugget zone could increase the strength. Hence the overall elongation of the joint is reduced. Subsequently, the relatively low ductility of the joints at high heat input conditions is a clear indication of the increase in strength of the weld nugget region of the heterogeneous joint zone.

Figures 16(a) and (b) demonstrate the contour plots of UTS and elongation against axial force and tool rotational speed. In this case, the UTS confirms a saddle (approximately) type variation characterized by the probable existence of multiple peaks within the parameter domain. Nevertheless, in the case of elongation, the variation is clearly of the peaking type with the existence of a unique peak within the domain. This observation once again indicates that the range of axial force values selected for the experimental trial is marginally shifted toward the upper side.

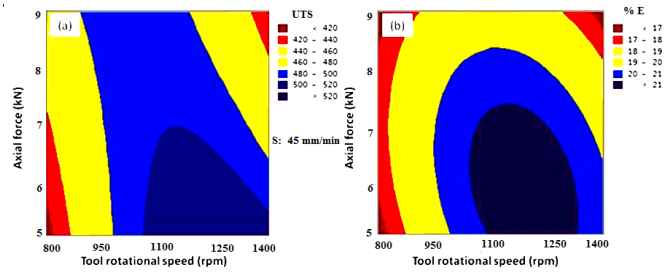

Fig. 16. Contour plot of: (a) UTS vs. tool rotational speed and axial force; (b) Elongation vs. tool rotational speed and axial force

4. OPTIMIZATION OF THE FSW PROCESS

The key features of the FSW process optimization including the imposed constraints are given in Table 6. With regard to tool rotational speed and welding speed, the upper and lower bounds that were considered for the experiment are taken as the constraints. However, the range of axial force considered is slightly towards the upper side, in order to avoid false convergence, no constraints are imposed for axial force. As UTS is the most significant objective and the elongation approximately follows the UTS, the UTS and elongation are assigned weights of four and one, respectively.

The composite desirability value of the problem is 0.9981. As the ideal value of desirability is unity, the composite desirability of 0.9981 indicates near-perfect optimization of the given problem. The optimum values of joint tensile strength and percentage elongation are 516 MPa and 21.57%, respectively at tool rotational speed of 1218 rpm, welding speed of 47 mm/min and axial force of 5.3 kN. The results of the optimization are validated using experimental trials. Three welds were made at the optimized parameter combination keeping the other factors such as tool profile, tool tilt angle, etc. as in the original investigation. The results of conformity trials agree reasonably well with the optimized UTS and percentage elongation with a maximum error of 6.2% and 7.3% in UTS and percentage elongation (% E), respectively.

Table 6
Constraints imposed for optimization

Goal	Weights	Constraints		
		Variables	Min	Max
Maximize UTS and % E	UTS – 4 and % E – 1	*N* rpm	800	1400
		S mm/min	30	60
		F	No Constraints	

5. CONCLUSIONS

In this work, 6 mm thick sheets of aluminium alloy AA 7068-T6 were friction stir welded using the response surface methodology – central composite face (RMS-CCF) centered experimental design. Second-order regression models were developed for tensile strength and elongation of the joints. Parametric optimization of the FSW process is carried out using the desirability function analysis.

- Friction stir welding (FSW) process could be used for the efficient joining of aluminium alloy AA7068-T6. A wider FSW parameter window could produce defect-free joints with acceptable joint properties.
- The tool rotational speed and welding speed have significant effect on the tensile strength and ductility of the joints. However, axial force is having relatively low interaction effect with tool rotational speed and welding speed on the tensile strength and ductility of the joints.
- FSW parameter combination that results in very low or very high heat generation produces joint with inferior properties. At moderate heat input welding conditions, the joint efficiency is found to be higher, but the lack of proper coalescence of material at the retreating side of the joint is critical in limiting the joint strength.
- The optimum values of joint tensile strength and percentage elongation are 516 and 21.57%, respectively at tool rotational speed of 1218 rpm, welding speed of 47 mm/min and axial force of 5.3 kN.

REFERENCES

[1] A.M. Khalil, I.S. Loginova, A.V. Pozdniakov, A.O. Mosleh, and A.N. Solonin, "Evaluation of the Microstructure and Mechanical Properties of a New Modified Cast and Laser-Melted AA7075 Alloy," *Materials*, vol. 12, no. 20, 2019. [Online]. Available: https://www.mdpi.com/1996-1944/12/20/3430.

[2] M. Minnicino, D. Gray, and P. Moy, "Aluminum alloy 7068 mechanical characterization," Army Research Lab Aberdeen Proving Ground MD Weapons and Materials Research, Tech. Rep., 2009.
[3] R.S. Mishra and Z. Ma, "Friction stir welding and processing," *Mater. Sci. Eng., R*, vol. 50, no. 1–2, pp. 1–78, 2005.
[4] M. Mohammadi-pour, A. Khodabandeh, S. Mohammadipour, and M. Paidar, "Microstructure and mechanical properties of joints welded by friction-stir welding in aluminum alloy 7075-T6 plates for aerospace application," *Rare Met*., pp. 1–9, 2016.
[5] P. Goel, A.N. Siddiquee, N.Z. Khan, M.A. Hussain, Z.A. Khan, M.H. Abidi, and A. Al-Ahmari, "Investigation on the effect of tool pin profiles on mechanical and microstructural properties of friction stir butt and scarf welded aluminium alloy 6063," *Metals*, vol. 8, no. 1, p. 74, 2018.
[6] N. Martinez, N. Kumar, R. Mishra, and K. Doherty, "Effect of tool dimensions and parameters on the microstructure of friction stir welded aluminum 7449 alloy of various thicknesses," *Mater. Sci. Eng. A*, vol. 684, pp. 470–479, 2017.
[7] W. Xu, H. Wang, Y. Luo, W. Li, and M. Fu, "Mechanical behavior of 7085-T7452 aluminum alloy thick plate joint produced by double-sided friction stir welding: Effect of welding parameters and strain rates," *J. Manuf. Processes*, vol. 35, pp. 261–270, 2018.
[8] M. Mehta, A. Arora, A. De, and T. DebRoy, "Tool geometry for friction stir welding – optimum shoulder diameter," *Metall. Mater. Trans. A*, vol. 42, no. 9, pp. 2716–2722, 2011.
[9] M. Jayaraman, R. Sivasubramanian, V. Balasubramanian, and A. Lakshminarayanan, "Application of RSM and ANN to predict the tensile strength of Friction StirWelded A319 cast aluminium alloy," *Int. J. Manuf. Res*., vol. 4, no. 3, pp. 306–323, 2009.
[10] S. Jannet, P. Mathews, and R. Raja, "Comparative investigation of friction stir welding and fusion welding of 6061 T6-5083 O aluminum alloy based on mechanical properties and microstructure," *Bull. Pol. Acad. Sci. Tech. Sci*., vol. 62, no. 4, 2014.
[11] K. Deepandurai and R. Parameshwaran, "Multiresponse optimization of FSW parameters for cast AA7075/SiCp composite," *Mater. Manuf. Processes*, vol. 31, no. 10, pp. 1333–1341, 2016.
[12] M.M. Krishnan, J. Maniraj, R. Deepak, and K. Anganan, "Prediction of optimum welding parameters for FSW of aluminium alloys AA6063 and A319 using RSM and ANN," *Mater. Today: Proc*., vol. 5, no. 1, pp. 716–723, 2018.
[13] M. Vahdati, M. Moradi, and M. Shamsborhan, "Modeling and Optimization of the Yield Strength and Tensile Strength of Al7075 Butt Joint Produced by FSW and SFSW Using RSM and Desirability Function Method," *Trans. Indian Inst. Met*., vol. 73, no. 10, pp. 2587–2600, 2020.
[14] G. Derringer and R. Suich, "Simultaneous optimization of several response variables," *J. Qual. Technol*., vol. 12, no. 4, pp. 214–219, 1980.
[15] G. Kumar, R. Kumar, and R. Kumar, "Optimization of process parameters of friction stir welded AA5082- AA7075 butt joints using resonance fatigue properties," *Bull. Pol. Acad. Sci. Tech. Sci*., vol. 68, no. 1, 2020, doi: 10.24425/bpasts.2020.131830.
[16] A.R. Rose, K. Manisekar, and V. Balasubramanian, "Effect of axial force on microstructure and tensile properties of friction stir welded AZ61A magnesium alloy," *Trans. Nonferrous Met. Soc. China*, vol. 21, no. 5, pp. 974–984, 2011.
[17] K. Jata, K. Sankaran, and J. Ruschau, "Friction-stir welding effects on microstructure and fatigue of aluminum alloy 7050-T7451," *Metall. Mater. Trans. A*, vol. 31, no. 9, pp. 2181–2192, 2000.
[18] F. Viana, A. Pinto, H. Santos, and A. Lopes, "Retrogression and re-ageing of 7075 aluminium alloy: microstructural characterization," *J. Mater. Process. Technol*., vol. 92, pp. 54–59, 1999.
[19] D. Godard, P. Archambault, E. Aeby-Gautier, and G. Lapasset, "Precipitation sequences during quenching of the AA 7010 alloy," *Acta Mater*., vol. 50, no. 9, pp. 2319– 2329, 2002.
[20] A.P. Reynolds, W. Tang, Z. Khandkar, J.A. Khan, and K. Lindner, "Relationships between weld parameters, hardness distribution and temperature history in alloy 7050 friction stir welds," *Sci. Technol. Weld. Joining*, vol. 10, no. 2, pp. 190–199, 2005.
[21] V.S. Gadakh and K. Adepu, "Heat generation model for taper cylindrical pin profile in fsw," *J. Mater. Res. Technol*., vol. 2, no. 4, pp. 370–375, 2013.
[22] K.K. Ramachandran, N. Murugan, and S.S. Kumar, "Performance analysis of dissimilar friction stir welded aluminium alloy AA5052 and HSLA steel butt joints using response surface method," *Int. J. Adv. Manuf. Technol*, vol. 86, no. 9, pp. 2373–2392, 2016.